

LIPG-promoted lipid storage mediates adaptation to oxidative stress in breast cancer

Cristina Cadenas¹, Sonja Vosbeck¹, Karolina Edlund¹, Katharina Grgas¹, Katrin Madjar², Birte Hellwig², Alshaimaa Adawy¹, Annika Glotzbach¹, Joanna D. Stewart¹, Michaela S. Lesjak¹, Dennis Franckenstein¹, Maren Claus³, Heiko Hayen⁴, Alexander Schriewer⁴, Kathrin Gianmoena¹, Sonja Thaler⁵, Marcus Schmidt⁶, Patrick Micke⁷, Fredrik Pontén⁷, Adil Mardinoglu⁸, Cheng Zhang⁸, Heiko U. Käfferlein⁹, Carsten Watzl¹, Saša Frank¹⁰, Jörg Rahnenführer², Rosemarie Marchan¹ and Jan G. Hengstler¹

¹Department of Toxicology, Leibniz-Research Centre for Working Environment and Human Factors at the TU Dortmund (IfAdo), Dortmund, Germany

²Department of Statistics, TU Dortmund University, Dortmund, Germany

³Department of Immunology, Leibniz-Research Centre for Working Environment and Human Factors at the TU Dortmund (IfAdo), Dortmund, Germany

⁴Department of Analytical Chemistry, Institute of Inorganic and Analytical Chemistry, University of Münster, Münster, Germany

⁵European Center for Angioscience (ECAS), Medical Faculty Mannheim of the University of Heidelberg, Tridomus C, Mannheim, Germany

⁶Department of Obstetrics and Gynecology, University Hospital Mainz, Mainz, Germany

⁷Department of Immunology Genetics and Pathology, Uppsala University, Uppsala, Sweden

⁸Science for Life Laboratory, KTH-Royal Institute of Technology, Stockholm, Sweden

⁹Center of Toxicology, Institute for Prevention and Occupational Medicine of the German Social Accident Insurance (IPA), Institute of the Ruhr University Bochum, Bochum, Germany

¹⁰Gottfried Schatz Research Center, Molecular Biology and Biochemistry, Medical University of Graz, Graz, Austria

Endothelial lipase (LIPG) is a cell surface associated lipase that displays phospholipase A1 activity towards phosphatidylcholine present in high-density lipoproteins (HDL). LIPG was recently reported to be expressed in breast cancer and to support proliferation, tumorigenicity and metastasis. Here we show that severe oxidative stress leading to AMPK activation triggers LIPG upregulation, resulting in intracellular lipid droplet accumulation in breast cancer cells, which supports survival. Neutralizing oxidative stress abrogated LIPG upregulation and the concomitant lipid storage. In human breast cancer, high LIPG expression was observed in a limited subset of tumours and was significantly associated with shorter metastasis-free survival in node-negative, untreated patients. Moreover, expression of *PLIN2* and *TXNRD1* in these tumours indicated a link to lipid storage and oxidative stress. Altogether, our findings reveal a previously unrecognized role for LIPG in enabling oxidative stress-induced lipid droplet accumulation in tumour cells that protects against oxidative stress, and thus supports tumour progression.

Key words: breast cancer, endothelial lipase, LIPG, lipid droplets, oxidative stress, *PLIN2*, *TXNRD1*

Abbreviations: ACC: Acetyl-CoA carboxylase; AMPK: AMP-activated protein kinase; BSA: Bovine serum albumin; DMEM: Dulbecco's modified medium; DOPC/PC-OA: 1,2-Dioleoyl-sn-glycero-3-phosphocholine; DPI: Diphenyleleiodonium; ER: Estrogen receptor; EV: Empty vector; FAS: *de novo* fatty acid synthesis; FASN: Fatty acid synthetase; FBS: Fetal bovine serum; FFA: Free fatty acids; FFPE: Formalin-fixed paraffin-embedded; HDL: High-density lipoproteins; IHC: Immunohistochemistry; LD: Lipid droplet; LIPG: Endothelial lipase; LPC: Lysophosphatidylcholine; LPL: Lipoprotein lipase; MDA: Malondialdehyde; MFS: Metastasis-free survival; MnTMPyP: Mn(111) tetrakis 1-methyl 4-pyridyl porphyrin pentachloride; NAC: N-acetyl-cysteine; OA: Oleic acid; OE: Overexpression; OIS: Oncogene-induced senescence; PC: Phosphatidylcholine; *PLIN2*: Perilipin 2; qPCR: quantitative realtime polymerase chain reaction; ROS: Reactive oxygen species; TAG: Triacylglycerides; TBARS: thiobarbituric acid reactive substances; TMA: Tissue microarray; TMRE: Tetramethylrhodamine methylester perchlorate; TOFA: 5-Tetradecyl-oxy-2-furoic acid; *TXNRD1*: Thioredoxin reductase 1

Joanna D. Stewart's current address is: University of Southampton, Highfield Campus, Southampton, United Kingdom

Adil Mardinoglu's additional affiliation is: Department of Biology and Biological Engineering, Chalmers University of Technology, Gothenburg, Sweden

Grant sponsor: The German Federal Ministry of Education and Research; **Grant number:** 01KU12161

DOI: 10.1002/ijc.32138

This is an open access article under the terms of the Creative Commons Attribution-NonCommercial License, which permits use, distribution and reproduction in any medium, provided the original work is properly cited and is not used for commercial purposes.

History: Received 6 Apr 2018; Accepted 19 Dec 2018; Online 17 Jan 2019

Correspondence to: Cristina Cadenas, Leibniz-Research Centre for Working Environment and Human Factors at the TU Dortmund (IfAdo), Ardeystr. 67, D-44139 Dortmund, Germany, Tel.: +49-2311084-392, Fax: +49-2311084-403, E-mail: cadenas@ifado.de

What's new?

Endothelial lipase (LIPG), a cell surface-associated lipase with multifaceted roles, is expressed on breast cancer cells, but its molecular function and clinical relevance remain unknown. Here the authors uncover a link between oxidative stress and LIPG upregulation and show that high LIPG expression is associated with shorter metastasis-free survival in women with node-negative breast cancer. The authors speculate that LIPG may favor metastasis by enabling stress adaptation through lipid droplet formation and protection of mitochondria.

Introduction

Lipid metabolism is highly relevant in cancer, as supported by numerous studies describing a role for lipids in cancer-related cellular processes, such as proliferation and invasion.^{1,2} The increased ability of cancer cells to synthesize lipids has led to the assumption that lipogenesis is the main mechanism by which cancer cells acquire fatty acids. Indeed, elevated expression and activity of enzymes involved in lipogenesis, such as fatty acid synthetase (FASN) are observed in tumour cells and correlate with cancer progression and worse prognosis in breast cancer patients.³ However, a recent study uncovered a pathway of fatty acid supply to cancer cells *via* lipoprotein lipase (LPL)-mediated lipolysis of extracellular lipoproteins.⁴ This showed that not all cancer cells rely exclusively on *de novo* fatty acid synthesis (FAS), but can also be fuelled by exogenous lipids. What determines the relative contribution of the lipogenic *vs.* the lipolytic pathways to the intracellular lipid pool is currently unknown.² Both pathways may be coupled to meet the increased demands of highly proliferating cancer cells for fatty acids as building blocks for more complex lipids. Alternatively, the metabolic fates of fatty acids derived from exogenous and endogenous sources may be different. The present study provides evidence that oxidative stress is a key factor shifting the balance towards increased activity of the lipolytic pathway by upregulating Lipase G, endothelial type (LIPG).

LIPG was originally identified in endothelial cells⁵ as a further member of the triglyceride lipase family⁶ and is a cell surface-associated lipase with predominantly phospholipase A1 activity. It cleaves phosphatidylcholine (PC) from high-density lipoproteins (HDL), thereby releasing free fatty acids (FFAs) and lysophosphatidylcholine (LPC), which can be taken up by cells.⁷ Due to its impact on HDL metabolism, LIPG has over past decades been primarily studied in the context of cardiovascular disease. Studies on a role for LIPG in cancer are scarce. We previously reported the upregulation of *LIPG* mRNA in a model of oncogene-induced senescence (OIS) in MCF-7 breast cancer cells, as part of the gene expression alterations that accompany senescence-associated remodelling of phospholipids.⁸ Later, Slebe and coworkers⁹ reported a broad and molecular subtype-independent expression of LIPG in breast cancer and a role for LIPG in providing lipids for tumour growth. Recently, Lo and coworkers¹⁰ described expression of LIPG in triple-negative breast cancer and a role for LIPG (independent of its catalytic activity) in promoting metastasis and invasiveness. While the discrepancy in the expression

pattern of LIPG in breast cancer still needs to be clarified, these reports suggest a multifaceted role of LIPG in tumour progression that deserves further studies. Remarkably, despite the essential functions of LIPG discovered in experimental models no significant association of LIPG with survival has been observed in human breast cancer.⁹

Our initial finding that LIPG is upregulated in oncogene-induced senescence – a state of hypermitotic arrest – prompted us to hypothesize that LIPG is necessary for survival under stress conditions, most probably due to its ability to supply cells with free fatty acids. Here, we report a new and proliferation-independent role for LIPG in oxidative stress-triggered lipid droplet accumulation that confers resistance to reactive oxygen species. Furthermore, in a systematic analysis of own and publicly available Affymetrix gene expression data we show that high *LIPG* mRNA expression is restricted to a small subset of breast tumours that are predominantly high grade and oestrogen receptor (ER)-negative. Finally, we demonstrate that high *LIPG* mRNA expression is significantly associated with shorter metastasis-free survival (MFS) in node-negative breast cancer.

Material and Methods**Chemicals**

5-Tetradecyl-oxy-2-furoic acid (TOFA), cerulenin, CoCl₂, N-acetyl-cysteine (NAC) and lapatinib, were obtained from Sigma Aldrich. GSK264220A, rotenone, and glutathione (GSH, reduced ethyl ester) were purchased from Cayman Chemical. The ROS scavenger MnTMPyP was purchased from Calbiochem/Merck and diphenyleiodonium (DPI) from Enzo Biochem.

Cell culture and treatments

The MCF-7 and the SKBR3 breast carcinoma cell lines were obtained from the American Type Culture Collection (ATCC, LGC Standards GmbH). MDA-MB-231, MDA-MB-468 and HCC1954 cells were purchased from the German Collection of Microorganisms and Cell Cultures (DSMZ). BT747 and T47D cells were obtained from Cell Lines Service (CLS). The MCF-7/NeuT cell line was generated and cultivated as described elsewhere.^{8,11,12} These cell lines were cultured at 37 °C in a humidified 5% CO₂ air atmosphere. MCF-7, MCF-7/NeuT, MDA-MB-231, MDA-MB-468 and SK-BR-3 cells were maintained in Dulbecco's modified medium (DMEM, 4.5 g/l glucose, PAN-Biotech), supplemented with 10% foetal bovine serum (FBS, PAN-Biotech). For the MCF-7/NeuT cell line tetracyclin-free FBS (PAN-Biotech) was used. BT-474 and T-47D cells were maintained in DMEM:F12, 10% FCS and

1% L-Glutamine (all from PAN-Biotech) and HCC1954 cells were cultivated in RPMI1640 with 10% FCS and 1% Sodium Pyruvate (Gibco). The HER2 wildtype and HER2 insYVMA MCF7 cell lines were established by retroviral transduction of MCF-7 cells with the corresponding plasmids¹³ and cultivated in RPMI with 10% FCS, 1% Pen/Strep and 1% L-Glutamine in the presence of puromycin (0.250 µg/mL). Cell exposure to hypoxia (1% O₂) was performed in a modular hypoxia/hyperoxia CO₂ incubator (CB53, Binder). The cell culture media was pre-equilibrated in the hypoxia incubator over night. Expression of LIPG and ACACA (the gene coding for the catalytic subunit alpha of Acetyl-CoA Carboxylase) was transiently downregulated using siRNA as described in Supplemental Material.

All cell lines were regularly tested for mycoplasma (Venor GeM Classic Mycoplasma Detection kit, Minerva Biolabs), and authenticated (DSMZ).

LIPG overexpression

MCF7 cells were transiently transfected with the full-length human LIPG cDNA cloned into pCMV/hygro-FLAG vector or with the empty vector (Sino Biological Inc.). Transfections were performed with the X-tremeGENE HP DNA transfection reagent according to the manufacturer's instructions (Sigma Aldrich) for 48 h. When applicable, 48 h after transfection cells were fed with either 800 µg high density lipoprotein (HDL, BioTrend) or 800 µg phospholipid (1,2-dioleoyl-sn-glycero-3-phosphocholine DOPC (PC-OA) (Avanti Polar Lipids) for a further 48 h. HDL was purchased 'ready to use'. Preparation of phospholipid vesicles and oleic acid/bovine serum albumin (OA/BSA) complex is described in Supplemental Material.

Immunoblotting

Standard immunoblot analysis was performed as described elsewhere.¹¹ Antibodies were diluted in 5% BSA/Tris-buffered saline Tween-20. Details about source, dilution and incubation conditions are provided in Supplemental Material. Protein signals were detected by enhanced chemiluminescence (PerkinElmer LAS). Quantification of Western blots was done with ImageJ. The density of the protein of interest was always adjusted to the density of the corresponding loading control.

Triacylglyceride quantification

Triglyceride levels in cells were quantified using the commercially available Triglyceride Quantification Kit (Abcam), according to the manufacturer's instructions. The fluorescence (Ex/Em 535/587 nm) was measured using a Tecan Infinite 200PRO plate reader (Tecan Group AG). The protein concentration of the extract was quantified using the Pierce BCA Protein Assay Kit (Thermo Fisher Scientific), according to the manufacturer's instructions, and used to normalize the fluorescent signal.

Quantification of mitochondrial membrane potential

Cells were incubated with tetramethylrhodamine methylester perchlorate (TMRE) (Invitrogen), for 20 min at 37 °C at a final concentration of 10 µM in medium containing serum. After washing with PBS, cells were trypsinized and the fluorescence of loaded TMRE (Ex/Em 545/575) was quantified in a plate reader (Tecan SpectraFluor Plus). For normalization, cell number was determined with a CASY cell counter (Innovatis AG/Roche).

Quantification of reactive oxygen species with the TBARS assay

Quantification of malondialdehyde (MDA) in cells (2x10⁷ cells collected in 1 mL PBS) was performed with the TBARS assay (Cayman Chemical) according to the colorimetric version of the manufacturer's instructions. Absorbance was read at 530–540 nm with a plate reader (Tecan SpectraFluor Plus).

Viability assay

Determination of the number of viable cells after treatments in multiwell plates was performed with the CellTiter-Blue[®] Cell Viability Assay (Promega) according to manufacturer's instructions. MCF-7 cells were incubated with the redox dye resazurin for 4 h. The fluorescent end product was measured in a Greiner 96 Flat Bottom Black Polystyrol 96-well plate (Ex/Em 540/590 nm) using a Tecan Infinite 200PRO plate reader (Tecan Group AG).

Immunofluorescence analysis

Cells were seeded on coverslips and, after the indicated treatments, a standard immunofluorescence protocol was performed. Details about source, dilution of the antibodies used and incubation conditions are provided in Supplemental Material. Coverslips were mounted and examined under a confocal laser scanning microscope (Olympus CLSM FV1000).

For visualization of lipid droplets, cells were stained after fixation and permeabilisation with either Oil Red O (Sigma Aldrich) for 30 min¹⁴ or with BODIPY[®] 493/503 (Life technologies) for 45 min. For visualization of actin filaments, cells were stained with rhodamine-labeled phalloidin (Invitrogen) for 45 min at room temperature.

Quantitative PCR

Total RNA extraction was performed with either the RNeasy Mini Kit (Qiagen) or the innuPREP RNA kit (Analytic Jena), according to the standard protocol of the manufacturer. RNA (2 µg) was transcribed to cDNA using the High-Capacity cDNA Reverse Transcription Kit (Applied Biosystems). Real-time quantitative PCR was performed with the Applied Biosystems ABI 7500 Fast Real-Time PCR System using the TaqMan technique. UBC was used as the reference gene for normalization. Taqman expression assays are found under Supplemental Material. Relative gene expression was calculated according to the 2- $\Delta\Delta$ Ct method.¹⁵

Heparin-release

For detection of the secreted, cell surface-bound fraction of LIPG, cells were washed with PBS and incubated in serum-free medium containing 10–25 U/mL heparin (Sigma Aldrich) for 16 h at 37 °C. The cell supernatants were collected in ice-cold tubes and after removal of dead cells by centrifugation, protein was precipitated using a standard ammonium sulfate precipitation procedure. Protein pellets were analysed by immunoblotting. Because no loading control was available for the immunoblotting of the supernatants, the signal intensity calculated with ImageJ was normalized to the total amount of protein of the corresponding cell cultures.

Immunohistochemistry of breast cancer tissue

Formalin-fixed paraffin-embedded (FFPE) tissue blocks from 258 node-negative, systemically untreated, breast cancer patients (See Table S1, Supporting Information with clinicopathological characteristics), who were operated between 1988 and 2000 at the Department of Obstetrics and Gynecology, Johannes Gutenberg University, Mainz, were used to construct a tissue microarray (TMA). The study was approved by the Research Ethics Committee of the University Medical Centre Mainz, Germany, and informed consent was obtained from all patients. Description of TMA construction and staining procedure is found in Supplemental Material. The stained TMA slides were scanned using a Hamamatsu NanoZoomer 2.0 whole slide scanner. LIPG cytoplasmic positivity was assessed by manual annotation of the scanned images at 10–40x magnification, based on the staining intensity which was categorized as (0) negative/weak, (1) moderate, and (2) strong. One score was obtained from the duplicate tissue cores representing each tumour.

Transcriptomics datasets

LIPG (probeset 219181_at), PLIN2 (209122_at) and TXNRD1 (201266_at) expression in human breast cancer were analysed in Affymetrix GeneChip HG U133 A or Plus 2.0 gene expression microarray datasets that were accessed from the Gene Expression Omnibus (GEO) web portal (<https://www.ncbi.nlm.nih.gov/geo/>).¹⁶ Duplicated patients were excluded. Clinicopathological characteristics and literature references for the analysed cohorts are summarized in Table S2, Supporting Information. Frozen robust multiarray analysis (fRMA)¹⁷ was used for the normalization of the Affymetrix data.

For additional analysis of LIPG expression, RNA-seq data from the Cancer Genome Atlas (TCGA) breast cancer dataset (BRCA) was used, including 1,125 tumour and 97 matched healthy tissue samples, accessed from the Genomic Data Commons (GDC) web portal (<https://gdc-portal.nci.nih.gov/>), as described.¹⁸ The TCGA BRCA dataset included 180 stage I, 609 stage II, 243 stage III, and 20 stage IV tumours (for 11 tumours, no information about stage was available).

Statistical analysis

All analyses of transcriptomics data were performed using R version 3.2.1 (R core team, 2015, <http://www.r-project.org/>). Categorization of clinical variables age, grade, pT stage, ER and HER2 status, dichotomization of LIPG expression, calculation of univariate and multivariate Cox analysis and likelihood ratio statistic are described in detail in Supplementary Material. Analyses of cell culture results were performed using GraphPad Prism, version 6 (La Jolla, CA, USA).

Results

LIPG enables cancer cells to use circulating lipoproteins as a nutrient source and promotes lipid storage

Previous work has shown that LIPG exerts phospholipase A1 activity towards high-density lipoprotein (HDL)-derived phosphatidylcholine (PC),¹⁹ releasing lipid products that become incorporated into intracellular PC and triacylglyceride (TAG) pools.⁷ Therefore, we investigated whether this also applies to breast cancer cells. First, endogenous expression of *LIPG* mRNA was measured in breast cancer cell lines of different subtypes: MCF-7 and T47D (ER+/HER2-), BT474 (ER+/HER2+), MDA-MB231 and MDA-MB-468 (ER-/HER2-) and SKBR3 and HCC1954 (ER-/HER2+). The results revealed the lowest *LIPG* mRNA levels in MCF-7 and the highest in MDA-MB-468 and HCC1954 cells (Fig. S1a, Supporting Information). This expression pattern was supported by Western blot analysis of the cell culture supernatants, but was not observed in cell lysates (Fig. S1b, Supporting Information), indicating that LIPG transcription is followed by secretion of the mature 68 kDa LIPG protein.

LIPG was overexpressed in MCF-7 cells using a vector containing *LIPG* tagged at the C-terminus with a FLAG epitope and overexpression was confirmed by qPCR, immunoblotting and immunofluorescence (Figs. S2a–S2c, Supporting Information). LIPG overexpression (LIPG-OE) in the presence of HDL resulted in an increase in intracellular TAG levels, as well as in the upregulation of the lipid droplet (LD)-coating protein Perilipin 2 (*PLIN2*), and LD accumulation (Fig. 1a) compared to cells transfected with vector alone (EV) and to non-transfected cells (FM control, Fig. S2d, Supporting Information). Besides HDL, also pure PC vesicles (PC esterified with oleic acid (PC-OA) served as a LIPG substrate, resulting in elevated levels of TAG, increased accumulation of LD, and upregulation of *PLIN2* expression (Fig. 1b). Addition of OA, one of the most abundant fatty acids released by LIPG,²⁰ to both LIPG-OE and EV-transfected cells resulted in comparable increases in TAG accumulation, *PLIN2* upregulation and LD accumulation irrespective of LIPG expression (Fig. 1c) as also shown in OA-treated parental MCF-7 cells (Fig. S2e, Supporting Information). LIPG overexpression in absence of substrate (Fig. 1d) did not elicit such a response, suggesting that both LIPG and substrate are required to increase the intracellular TAG pool. These results demonstrate that MCF-7 breast cancer cells are able to incorporate exogenous free fatty acids

into TAGs, but only LIPG expression renders them capable of using HDL or PC as a fatty acid source.

Given that LIPG overexpression results in intracellular lipid storage in MCF-7 cells, we investigated whether upregulation of endogenous LIPG by sustained oncogenic signalling in MCF-7/NeuT cells was also associated with elevated intracellular TAG. Previously, we observed upregulation of *LIPG* mRNA in MCF-7/NeuT breast cancer cells which conditionally overexpress an oncogenic variant of the rat Her2/ErbB2/Neu receptor tyrosine kinase (NeuT), leading to oncogene-induced senescence (OIS).⁸ After demonstrating doxycycline (dox)-triggered expression of NeuT, together with the EGFP reporter and the characteristic morphological changes associated with premature senescence, such as cell enlargement and flattening (Figs. 2a and 2b), we confirmed a more than tenfold upregulation of *LIPG* mRNA by qPCR (Fig. 2c and Fig. S3a, Supporting Information). LIPG protein was detected in the supernatant of the senescent MCF-7/NeuT (+dox), but not in control (-dox) cells, as the 68 kDa full-length glycosylated form together with its 40 kDa cleavage product (Fig. 2d and Fig. S3b, Supporting Information). This demonstrates that induction of LIPG transcription is followed by secretion of LIPG protein. Cytoplasmic LIPG protein levels were not increased by dox treatment (Figs. S3c-S3d, Supporting Information). Thus, the inducible 68 kDa LIPG protein pool becomes readily secreted and is only detected in the extracellular fraction. No other members of the triglyceride lipase family were shown to be significantly up or downregulated upon NeuT induction in MCF7/NeuT cells (Table S3, Supporting Information).

MCF-7/NeuT cells examined 6d after NeuT induction (6d + dox) showed a threefold increase in TAG levels compared to control cells (6d-dox) (Fig. 2e). Consistently, *PLIN2* was also upregulated in MCF-7/NeuT cells upon NeuT induction (Fig. 2f). Blockage of LIPG activity with the LIPG inhibitor GSK264220A²¹ significantly reduced intracellular TAG levels (Fig. 2g) and LD accumulation (Fig. 2h) in MCF-7/NeuT cells. Thus, the increased triglyceride levels observed in NeuT-induced senescence depend partially on LIPG activity.

LIPG expression is upregulated in oxidative stress conditions that compromise *de novo* fatty acid synthesis

Subsequent analyses aimed to identify stimuli that are able to upregulate LIPG. Upregulation of LIPG in MCF-7/NeuT cells after induction of oncogenic HER2 (NeuT) suggested that LIPG could be a target of HER2. However, upregulation of *LIPG* by HER2 has not been reported in other studies. Therefore, we investigated LIPG expression in MCF-7 cells stably transfected with wildtype HER2 or with a HER2 mutant containing a YVMA insertion in the kinase domain (A775_G776) that also enhances tyrosine kinase activity^{13,22} and activates AKT, MEK1/2-ERK1/2 and P38 signalling pathways as described for NeuT^{11,12} (Fig. S4a, Supporting Information). qPCR analysis did not show an upregulation of *LIPG* in the HER2 insYVMA or the HER2 wildtype overexpressing MCF-7 cells (Fig. S4b, Supporting Information).

This suggests that *LIPG* expression is not generally triggered by HER2. Rather, *LIPG* expression in MCF-7/NeuT cells may be the consequence of a metabolic reprogramming induced by the hyperactive NeuT.

One further hypothesis was that a compromised *de novo* lipogenesis may induce pathways of exogenous lipid uptake in breast cancer cells. Therefore, we pharmacologically inhibited *de novo* FAS in MCF-7 cells by the acetyl CoA carboxylase (ACC) inhibitor 5-tetradecyl-oxy-2-furoic acid (TOFA)²³ and by the FASN inhibitor cerulenin (Fig. 3a). Inhibition by TOFA but not by cerulenin resulted in a significant upregulation of *LIPG* mRNA (Fig. 3b) in a concentration-dependent manner (Fig. S5a, Supporting Information). This suggests that impairing ACC activity may determine *LIPG* upregulation. Silencing of the ACC catalytic subunit *ACACA* via transfection with siRNA (Fig. S5b, Supporting Information) also resulted in a slight upregulation of *LIPG* mRNA (Fig. S5c, Supporting Information) and supported the hypothesis that LIPG compensates a diminished *de novo* FAS.

Accordingly, we next studied whether ACC is inhibited in senescent MCF-7/NeuT cells. Different stress conditions, including reactive oxygen species (ROS), activate the AMP-kinase (AMPK), which in turn phosphorylates and inhibits ACC (Fig. 3a).^{24,25} An increase in ROS generation has been demonstrated in MCF-7/NeuT and other models of oncogene-induced senescence (OIS),^{11,26} including lipid peroxides¹¹ as well as superoxide anions and hydrogen peroxide.²⁶ Thus, as expected, we confirmed the previously observed upregulation of thioredoxin reductase (TXNRD1)¹¹ (Fig. 3c) and increased levels of thiobarbituric acid reactive substances (TBARS) (Fig. 3d) as measures of ROS-mediated lipid peroxidation and demonstrated phosphorylation (activation) of AMPK (Fig. 3e) and phosphorylation (inhibition) of ACC (Fig. 3f) in senescent MCF-7/NeuT cells. Together, these data suggest that oxidative stress is a biological context in which fatty acid synthesis is inhibited, and the resulting compensatory induction of LIPG occurs.

LIPG protects from mitochondrial dysfunction under metabolic stress conditions

Published studies have shown that fatty acids derived from intracellular LD-lipolysis support cells during starvation,²⁷ and are delivered to mitochondria.²⁸ This is supported by the association of PLIN2-positive LDs with mitochondria.^{28,29} We confirmed the relevance of LDs in cell survival by monitoring cell growth during the course of a feeding-starvation experiment. As shown in Figure S6a, Supporting Information, cells fed with OA had a survival advantage during starvation. To study a possible contribution of LDs in mitochondrial integrity, tetramethylrhodamine methyl ester perchlorate (TMRE), which only accumulates in functional mitochondria with transmembrane potential ($\Delta\psi_m$), was monitored. TMRE levels were higher in cells that had lipid stores available during starvation (Fig. S6b, Supporting Information).

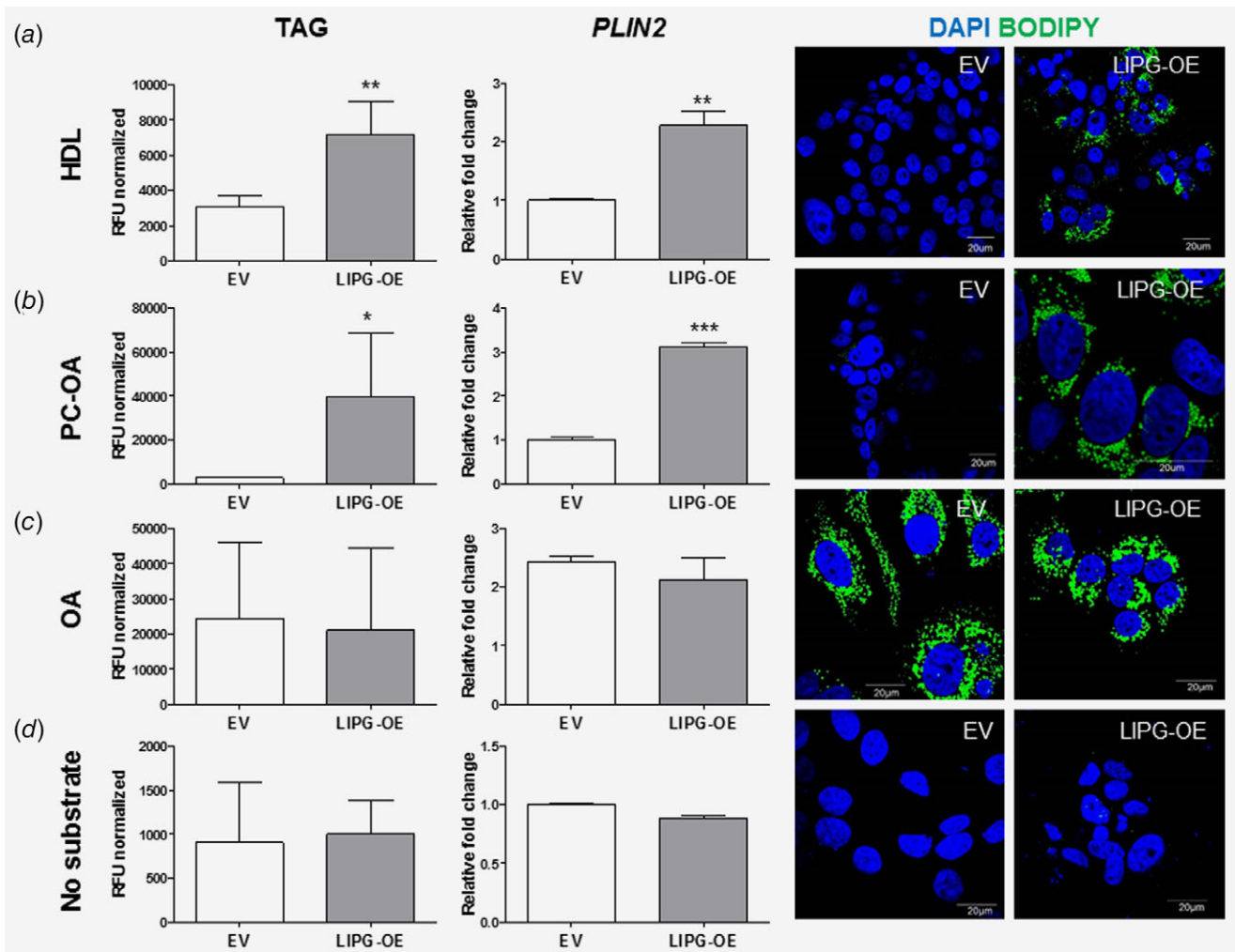


Figure 1. LIPG overexpression in MCF-7 cells results in intracellular lipid storage. MCF-7 cells were transfected with a LIPG construct (LIPG-OE) or an empty vector (EV) and incubated for 48 h with (a) 800 μ g HDL, (b) 800 μ g PC-OA in serum-free DMEM, (c) 800 μ g oleic acid (OA) complexed to bovine serum albumin and (d) no substrate. Intracellular triacylglyceride (TAG) levels were quantified with the triglyceride quantification assay kit. *PLIN2* mRNA levels were analysed by qPCR. Lipid droplets were visualized with Bodipy 493/503 staining (green). Nuclei were stained with DAPI (blue). The bars represent the mean \pm SEM and pictures are representative of three independent experiments. * $p < 0.05$; ** $p < 0.01$; *** $p < 0.001$, unpaired two-tailed Student's t-test. [Color figure can be viewed at wileyonlinelibrary.com]

We next investigated whether LIPG-mediated lipid supply confers a survival advantage to cells. To this end we explored whether LIPG-mediated LD accumulation supports mitochondria under conditions of compromised FAS. When blocking *de novo* FAS with TOFA in LIPG-OE and EV transfected cells fed with PC-OA, mitochondrial integrity was higher in LIPG overexpressing cells than in control cells (Fig. 3g), supporting that LIPG provides a survival advantage once endogenous FAS is limited.

Upregulation of *LIPG* by CoCl_2 contributes to lipid storage and adaptation to oxidative stress and is abrogated by ROS scavengers

To investigate further oxidative stress stimuli, we used the hypoxia-mimicking and ROS-inducing agent cobalt chloride (CoCl_2). Exposure of MCF-7 cells to CoCl_2 resulted in AMPK phosphorylation in a concentration-dependent manner (Fig. 4a).

Although phosphorylation of the AMPK-target ACC was not increased, total ACC protein levels decreased significantly (Fig. 4b) in agreement with studies showing that AMPK can also regulate ACC at the transcriptional level, repressing its promoter activity *via* NRF-1.³⁰ *LIPG* was upregulated more than fivefold at high concentrations of CoCl_2 (0.9 mM) (Fig. 4c). In line with the ROS-generating effect of CoCl_2 , which has been reported to increase superoxide production by mitochondria,³¹ *TXNRD1* mRNA was also induced (Fig. 4c). CoCl_2 also led to the upregulation of *PLIN2* mRNA (Fig. 4c) and to increased levels of TAG and LDs (Fig. 4d). The contribution of LIPG to CoCl_2 -triggered lipid storage was demonstrated by showing restoration of basal TAG levels and concomitant reduction of the amount of LDs (Figs. 4e and 4f) upon inhibition of LIPG with GSK264220A. Furthermore, also knockdown of LIPG, which showed >80% reduction of LIPG mRNA and loss of the secreted 68 kDa LIPG

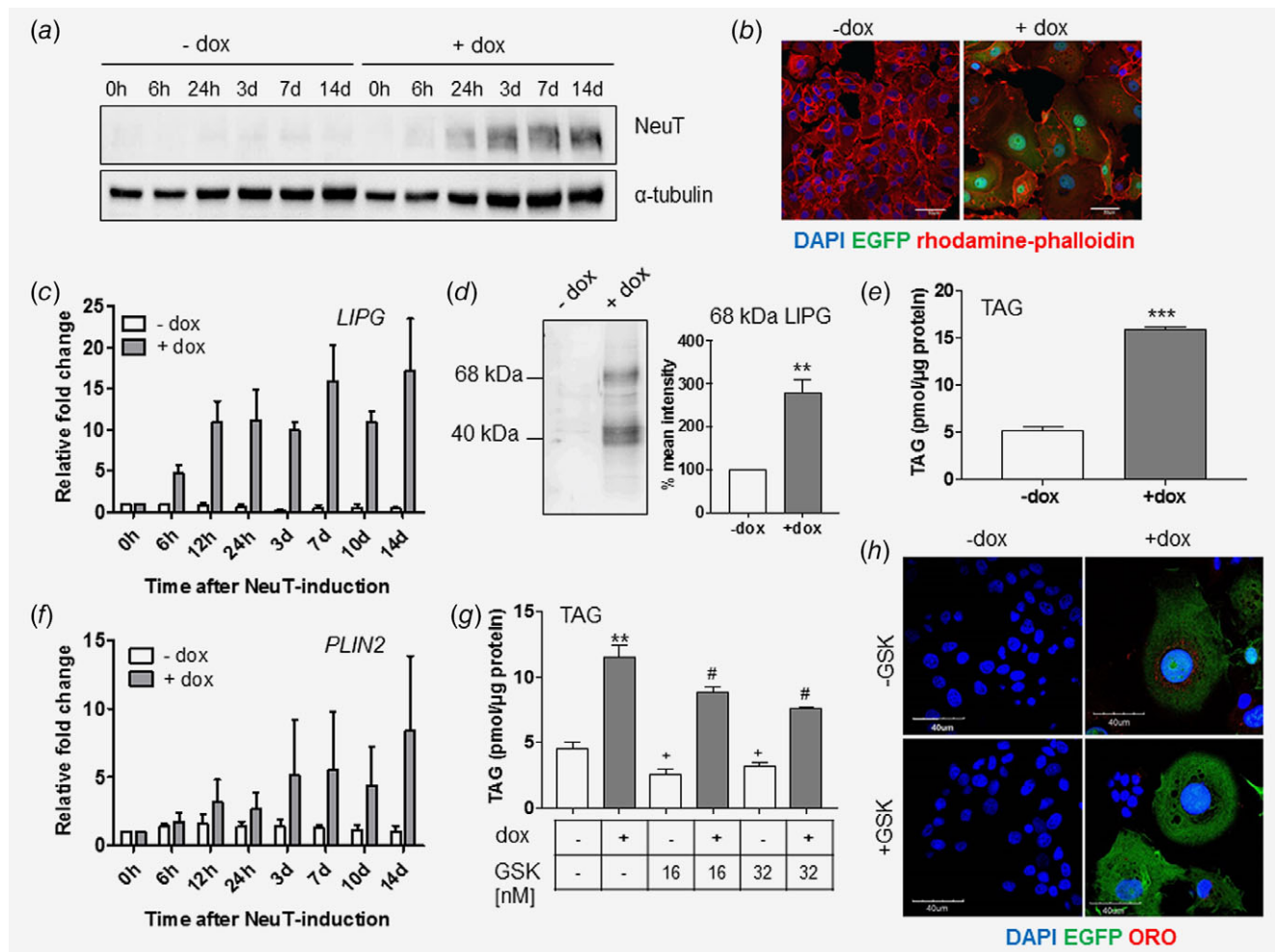


Figure 2. Upregulation of LIPG in NeuT-induced senescence contributes to lipid storage. (a) Representative Western blot showing expression of the NeuT oncogene in MCF-7/NeuT cells treated with doxycycline (+dox) or untreated (-dox) at different time points. (b) Immunofluorescence illustrating senescence-associated morphological changes and co-induction of the reporter EGFP (green) upon dox treatment. The actin cytoskeleton was stained with rhodamine phalloidin (red); nuclei were stained with DAPI (blue); scale bar: 50 μ m. (c) qPCR showing *LIPG* mRNA expression in MCF-7/NeuT cells incubated with/without dox during the indicated time periods. Data represent the mean fold change in mRNA relative to time point 0 h \pm SEM (n = 3). (d) Representative Western blot showing the 68 kDa LIPG protein and its 40 kDa cleavage product in supernatants of MCF-7/NeuT cells (6d -/+ dox) incubated with heparin and densitometric quantification of the 68 kDa LIPG band from Western blots signals of three independent experiments (see also Fig. S3, Supporting Information). (e) Quantification of cellular triacylglycerides (TAG) in MCF-7/NeuT cells cultivated for 7d with/without dox (time point of high *LIPG* expression). (f) *PLIN2* mRNA expression, analysed by qPCR as in (c). (g) Quantification of cellular triacylglycerides (TAG) in MCF-7/NeuT cells cultivated for 6d with/without dox (\pm dox) in the presence or absence of 16 nM or 32 nM of the LIPG inhibitor GSK264220A. (h) Oil Red O (ORO) staining (red) to visualize lipid droplets in MCF-7/NeuT cells treated for 6d-7d \pm dox in the presence or absence of the LIPG inhibitor GSK264220A (32 nM); blue: DAPI green: EGFP. Scale bar: 40 μ m. All bar plots represent the mean \pm SEM of three independent experiments. ** p < 0.01; *** p < 0.001 (for comparison between -dox and + dox incubated cells); # p < 0.05 (dox + GSK264220A-incubated vs. dox only-incubated cells); * p < 0.05 (GSK264220A-treated vs. untreated cells). p -Values were calculated by unpaired two-tailed Student's t-test. [Color figure can be viewed at wileyonlinelibrary.com]

protein led to a decreased cellular TAG content (Figs. S7a-S7d, Supporting Information). Moreover, it prevented upregulation of LIPG upon exposure to CoCl_2 (Fig. 4g) and led to a significant decrease in cell viability (Fig. 4h), demonstrating a role for LIPG in adaptation to oxidative stress.

Because CoCl_2 also acts as a hypoxia mimetic, we explored the possible upregulation of LIPG by hypoxia. We observed no hypoxia-specific upregulation of LIPG (Fig. S8,

Supporting Information), rather a cell density-dependent downregulation. A similar pattern was shown for *TXNRD1*. Hypoxia-dependent upregulation of *PLIN2* accompanied the increased expression of the hypoxia marker *VEGF* (Fig. S8, Supporting Information), which altogether suggests a hypoxia-triggered LD accumulation in a LIPG-independent manner. Incubation of cells with H_2O_2 also led to a slight but significant induction of LIPG and *TXNRD1*

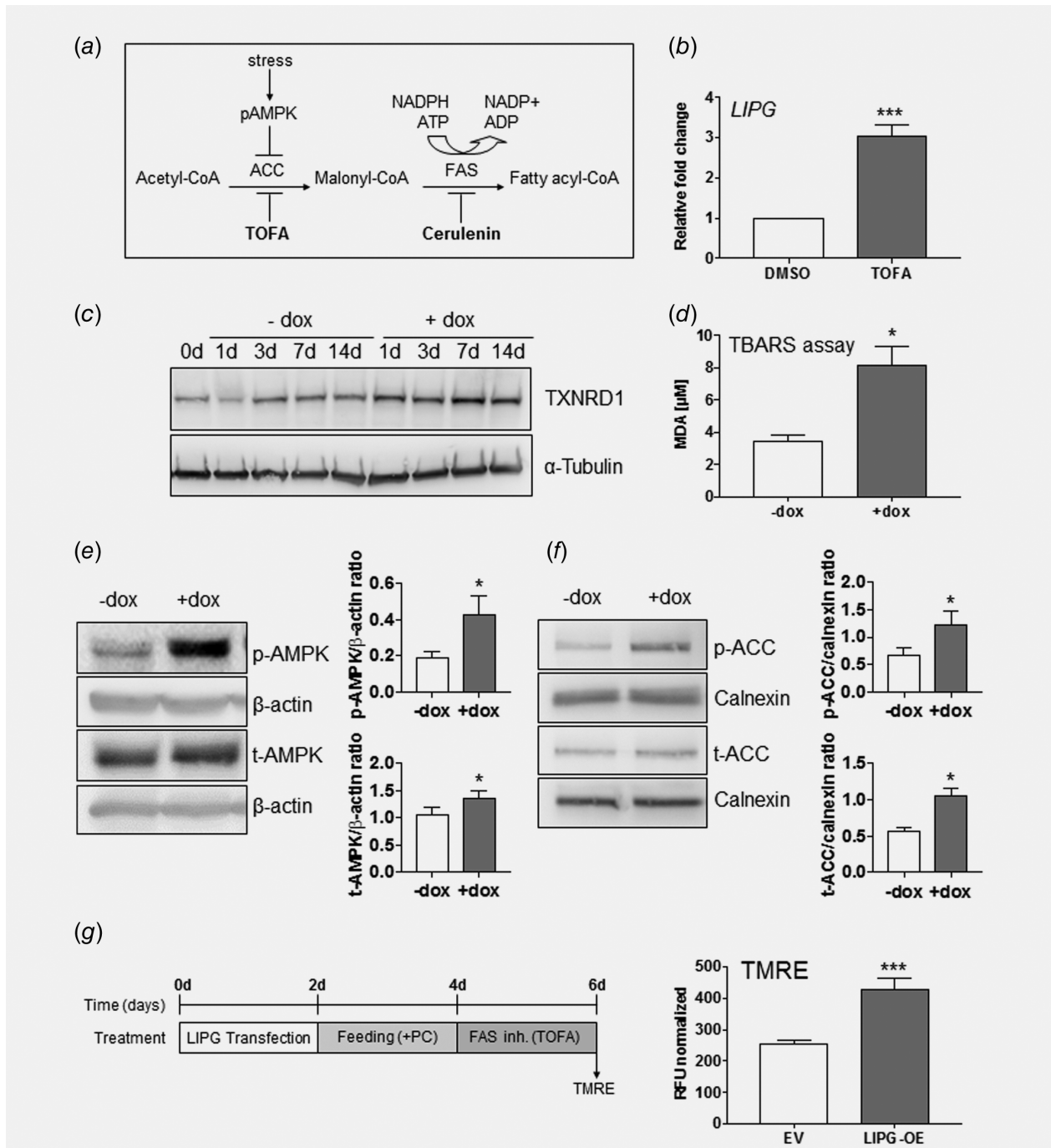


Figure 3. LIPG becomes upregulated upon cellular stress-mediated inhibition of *de novo* fatty acid synthesis (FAS). (a) Schematic illustration of the initial steps of *de novo* fatty acid synthesis, regulation of acetyl-CoA carboxylase (ACC) by AMPK, and pharmacological inhibition by TOFA and cerulenin. (b) qPCR analysis of *LIPG* mRNA expression in MCF-7 cells incubated for 24 h with 6 μM TOFA (n = 4). (c) Representative Western blot showing protein levels of TXNRD1 in MCF-7/NeuT cells incubated with/without dox at the indicated time points. (d) TBARS assay showing levels of ROS in cellular extracts of MCF-7/NeuT cells incubated 7d with/without dox (n = 3). (e) Representative Western blots showing the phosphorylation status of AMPK in MCF-7/NeuT cells (6d with/without dox) and densitometric quantification of the ratios of phospho-AMPK (p-AMPK) and total-AMPK (t-AMPK) to β-actin from Western blot signals of three independent experiments. (f) Representative Western blot showing the phosphorylation status of ACC in MCF-7/NeuT cells (6d with/without dox) and densitometric quantification of the ratios of phospho-ACC (p-ACC) and total-ACC (t-ACC) to calnexin from Western blot signals of three independent experiments. Bars indicate mean ± SEM. ***p < 0.001; *p < 0.05, unpaired two-tailed Student's t-test. (g) Mitochondrial integrity of cells transfected with LIPG or empty vector (EV), fed with LIPG substrate (PC) and subsequently treated with TOFA to block fatty acid synthesis. The bar diagrams represent the mean ± SEM of three independent experiments. ***p < 0.001, unpaired two-tailed Student's t-test.

(Fig. S9a, Supporting Information), and treatment with rotenone, which results in superoxide generation, led to an even higher upregulation of *LIPG* and *TXNRD1* (Fig. S9b, Supporting Information), again reinforcing the link between *LIPG* and oxidative stress.

Altogether, these results strongly support the concept that oxidative stress upregulates *LIPG* as an alternative lipid supply pathway in breast cancer cells where *de novo* FAS is compromised by ROS.

In view of these results, we tested the ability of the ROS scavenger N-acetyl-cysteine (NAC) to counteract the effects of CoCl_2 . Addition of NAC abrogated CoCl_2 -triggered phosphorylation of AMPK (Fig. 4i). Furthermore, both *LIPG* and *PLIN2* induction were prevented in the presence of NAC (Fig. 4j). *TXNRD1* expression also decreased to control levels, confirming efficient scavenging of ROS (Fig. 4j). Moreover, TAG levels were normalized upon NAC treatment (Fig. 4k) and no accumulation of LDs was observed (Fig. 4l). Supplementing CoCl_2 -treated MCF-7 cells with GSH partially prevented *LIPG* and *TXNRD1* upregulation as well (Fig. S10, Supporting Information). Hence, counteracting oxidative stress prevents the upregulation of *LIPG* as well as *LIPG*-mediated lipid storage.

In senescent MCF-7/NeuT cells neither NAC nor the superoxide scavenger Mn(111) tetrakis 1-methyl 4-pyridyl porphyrin pentachloride (MnTMPyP) nor diphenyleneiodonium chloride (DPI), an inhibitor of NADPH oxidase-like flavoenzymes, which efficiently scavenged ROS in other models of OIS,^{32,33} counteracted oxidative stress (Figs. S11a–S11c, Supporting Information). Accordingly, *LIPG* and *TXNRD1* levels remained high (Figs. S11a–S11c, Supporting Information). Only the inhibition of the tyrosine kinase activity of HER2/NeuT with lapatinib markedly decreased *LIPG* levels and slightly diminished *TXNRD1* mRNA. (Fig. S11d, Supporting Information). Thus, oxidative stress caused by the constitutively active NeuT in MCF-7/NeuT cells cannot be efficiently scavenged by conventional antioxidants. Only by antagonizing its tyrosine kinase activity was *LIPG* upregulation inhibited. A striking observation was the strong upregulation of *LIPG*, *PLIN2*, and *TXNRD1* in control cells (–dox, non-senescent) upon treatment with DPI and MnTMPyP. This suggests that *LIPG* upregulation also occurs in response to reductive stress, and is thus responsive to general disturbances in the cellular redox state.

High *LIPG* expression associated with shorter metastasis-free survival in human node-negative breast cancer

Recent reports indicate the relevance of *LIPG* in human breast cancer.^{9,10} However, discrepancies between the studies with regard to *LIPG* expression remained unclarified. We analysed *LIPG* gene and protein expression in our previously established breast cancer cohort (Mainz cohort, GSE11121) of node-negative breast cancer patients who were untreated in both neoadjuvant and adjuvant settings.^{34,35} *LIPG* mRNA (Affymetrix probeset 219181_at) revealed a bimodal expression distribution, where a

small subset of tumours expressed high *LIPG* levels (Fig. 5a and Fig. S12a, Supporting Information). To validate this finding, we explored additional, publicly available breast cancer cohorts. A similar distribution, with only a relatively small subset of tumours expressing high levels of *LIPG*, was also observed in three publicly available node-negative, untreated breast cancer cohorts, as well as in several datasets of patients who received adjuvant or neoadjuvant therapy (Fig. 5a and Figs. S12a–S12c, Supporting Information). Comparing *LIPG* levels analysed by Affymetrix gene array and qPCR for a selection of tumours from the Mainz cohort, for which RNA was available, revealed a strong correlation between the two methods (Pearson $r = 0.96$, $p < 0.001$) (Fig. 5b) and excluded that the observed expression pattern was due to probeset-dependent effects. Moreover, also in the TCGA breast cancer dataset, including data from 1,125 specimens analysed with RNA sequencing (<https://tcga-data.nci.nih.gov/>) was only a small subset of breast tumours with high *LIPG* expression observed (Fig. S13a, Supporting Information), further indicating that high *LIPG* expression is rare in human breast cancer.

In the Mainz cohort, higher *LIPG* expression was significantly associated with shorter MFS in a univariate Cox analysis (Table S4, Supporting Information). The small subset of patients with tumours expressing high *LIPG* levels showed significantly shorter MFS, illustrated by a Kaplan–Meier plot (Fig. 5c, left panel). In contrast, a recent study⁹ investigating *LIPG* protein levels in a TMA of 439 breast cancer patients using immunohistochemistry (IHC), reported high and ubiquitous expression of *LIPG*, and no association with outcome. Interestingly, when a TMA including the patients of the Mainz cohort was immunostained using the same antibody as Slebe *et al.*,²⁹ broad cytoplasmic *LIPG* expression was also observed (Fig. 5d, upper and lower left panel), and there was no association of *LIPG* positivity with clinicopathological parameters (Table S5, Supporting Information) or MFS (Fig. 5d, lower middle panel). Importantly, we observed no correlation between cytoplasmic *LIPG* protein staining by IHC with this antibody and mRNA levels (Fig. 5d, lower right panel). This is in line with the results obtained *in vitro*, showing that not cytoplasmic but secreted *LIPG* reflects mRNA levels.

To further validate the association of high *LIPG* mRNA expression with MFS, three additional node-negative, untreated breast cancer datasets (GSE2034 $n = 286$; Transbig: GSE6532 $n = 84$ and GSE7390 $n = 196$; and GSE5327 $n = 58$) were analysed. As observed in the Mainz cohort, a significantly shorter MFS was observed for high *LIPG*-expressing tumours in the Transbig cohort (Table S4, Supporting Information), as well as in the combined node-negative dataset (Table 1), illustrated by Kaplan–Meier plots (Fig. 5c, right panel). In the combined node-negative dataset, high *LIPG* expression correlated with ER negative status ($p < 0.001$) and high tumour grade ($P = 0.014$) (Table S6, Supporting Information). Interestingly, in a multivariate Cox analysis, *LIPG* was associated with worse prognosis, independent of grade, stage, age, ER-, and HER2 status (Table 1).

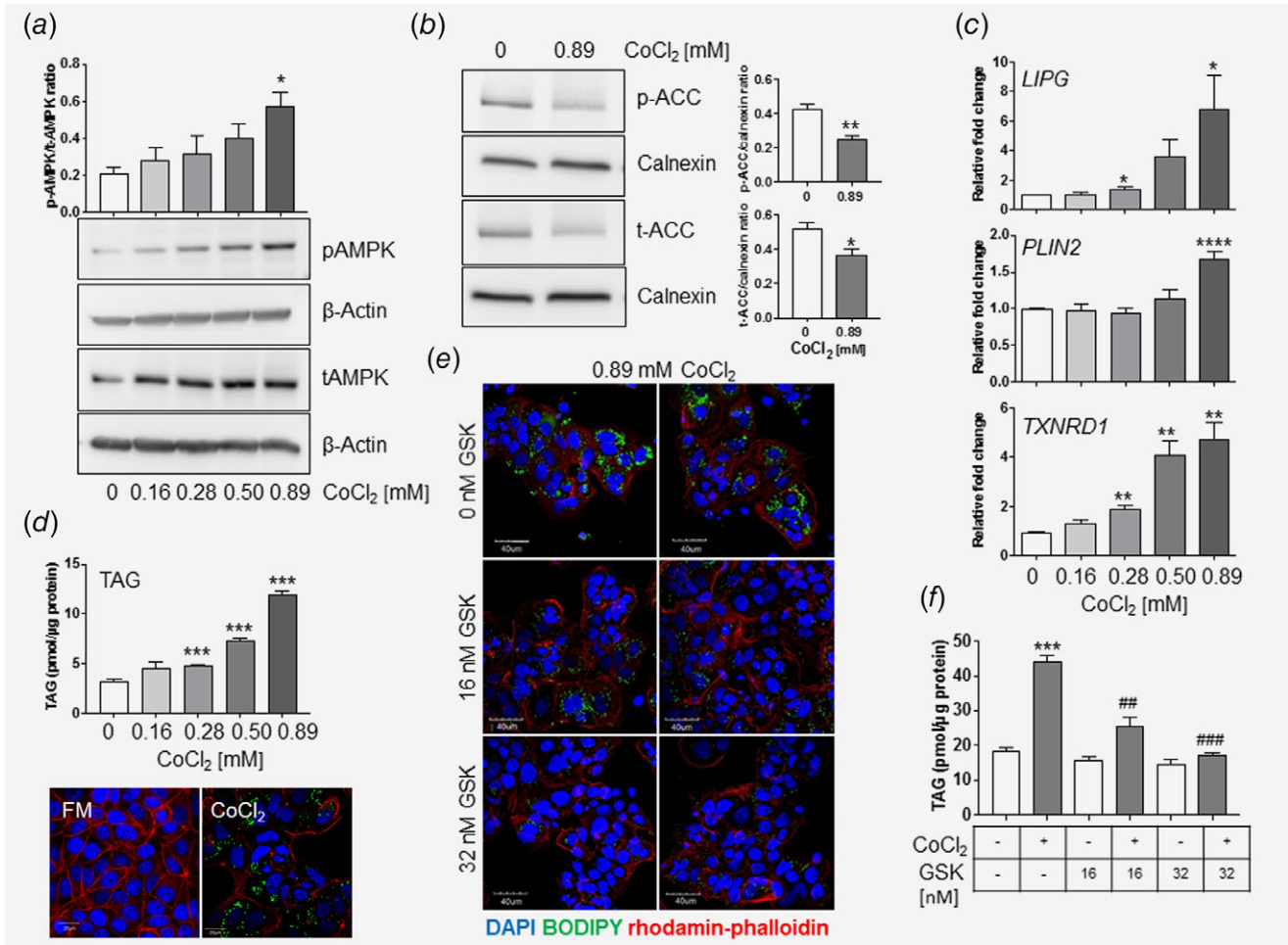


Figure 4. Upregulation of *LIPG* by CoCl₂ contributes to lipid storage and adaptation to oxidative stress and is abrogated by ROS scavengers. (a) Representative Western blot showing AMPK phosphorylation in MCF-7 cells exposed to different concentrations of CoCl₂ for 24 h and densitometric quantification of the ratio (phospho-AMPK/total-AMPK) from Western blot signals of three independent experiments. (b) Representative Western blot showing ACC phosphorylation in MCF-7 cells exposed to 0.89 mM of CoCl₂ for 24 h and densitometric quantification of the ratios (p-ACC and t-ACC to calnexin) from Western blot signals of three independent experiments. (c) qPCR analysis showing *LIPG*, *PLIN2* and *TXNRD1* mRNA levels in MCF-7 cells treated for 24 h with the indicated concentrations of CoCl₂. (d) Quantification of triacylglycerides (TAG) in MCF-7 cells exposed for 24 h to the indicated concentrations of CoCl₂ and visualization of lipid droplets by BODIPY 493/503 staining (green) in 0.89 mM CoCl₂-treated and untreated (FM) MCF-7 cells; red: Rhodamine phalloidin staining of the actin cytoskeleton; blue: DAPI. Scale bars: 20 μm. (e) Visualization of lipid droplets in MCF-7 cells exposed to 0.89 mM CoCl₂ for 24 h in the presence or absence of 16 nM or 32 nM of the LIPG inhibitor GSK264220A. red: Rhodamine phalloidin staining of the actin cytoskeleton; blue: DAPI. Scale bars: 40 μm. (f) Quantification of TAGs in CoCl₂-treated MCF-7 cells in the presence or absence of 16 nM or 32 nM GSK264220A (duplicates are shown). (g) qPCR analysis showing *LIPG* mRNA levels in MCF-7 cells after transfection with scrambled si-RNA as a negative control (si-neg) and two different si-RNA oligos targeting *LIPG* (si-*LIPG*-A and si-*LIPG*-B), compared to FM (full media, non-transfected control) and Lipo (Lipofectamine only, mock-transfected) and subsequent 24 h-exposure to CoCl₂. (h) Cell Titer Blue viability assay showing cell survival after three more days under the same conditions as in (g). Bar diagrams represent the mean ± SEM of three independent experiments; **p* < 0.05; ***p* < 0.01; ****p* < 0.0001 for comparison of each of the siRNAs with the negative control (scramble, si-neg). ####*p* < 0.0001; ###*p* < 0.001 for comparisons to untreated cells (FM). *p*-Values were calculated by unpaired two-tailed Student's *t*-test. (i) Representative Western blot showing AMPK phosphorylation in MCF-7 cells exposed to 0.5 mM or 0.89 mM CoCl₂ alone or in the presence of 20 mM NAC for 24 h and densitometric quantification of the ratio (phospho-AMPK/total-AMPK) from Western blot signals of three independent experiments. (j) qPCR analysis showing mRNA levels of *LIPG*, *PLIN2* and *TXNRD1* in MCF-7 cells exposed to CoCl₂ in the presence or absence of 20 mM NAC. (k) Quantification of cellular TAGs in MCF-7 cells exposed to CoCl₂ in the presence or absence of 20 mM NAC. (l) Visualization of lipid droplets by BODIPY 493/503 (green) in CoCl₂-treated in MCF-7 cells in the presence or absence of 20 mM NAC; red: Rhodamine phalloidin staining of the actin cytoskeleton; blue: DAPI. Scale bars: 40 μm. All bar diagrams represent the mean ± SEM of three independent experiments. **p* < 0.05; ***p* < 0.01; ****p* < 0.001 (CoCl₂-treated vs. untreated cells); #*p* < 0.05; ##*p* < 0.01; ###*p* < 0.001 (NAC-treated or GSK264220A-treated vs. untreated cells). *p*-Values were calculated by unpaired two-tailed Student's *t*-test. [Color figure can be viewed at wileyonlinelibrary.com]

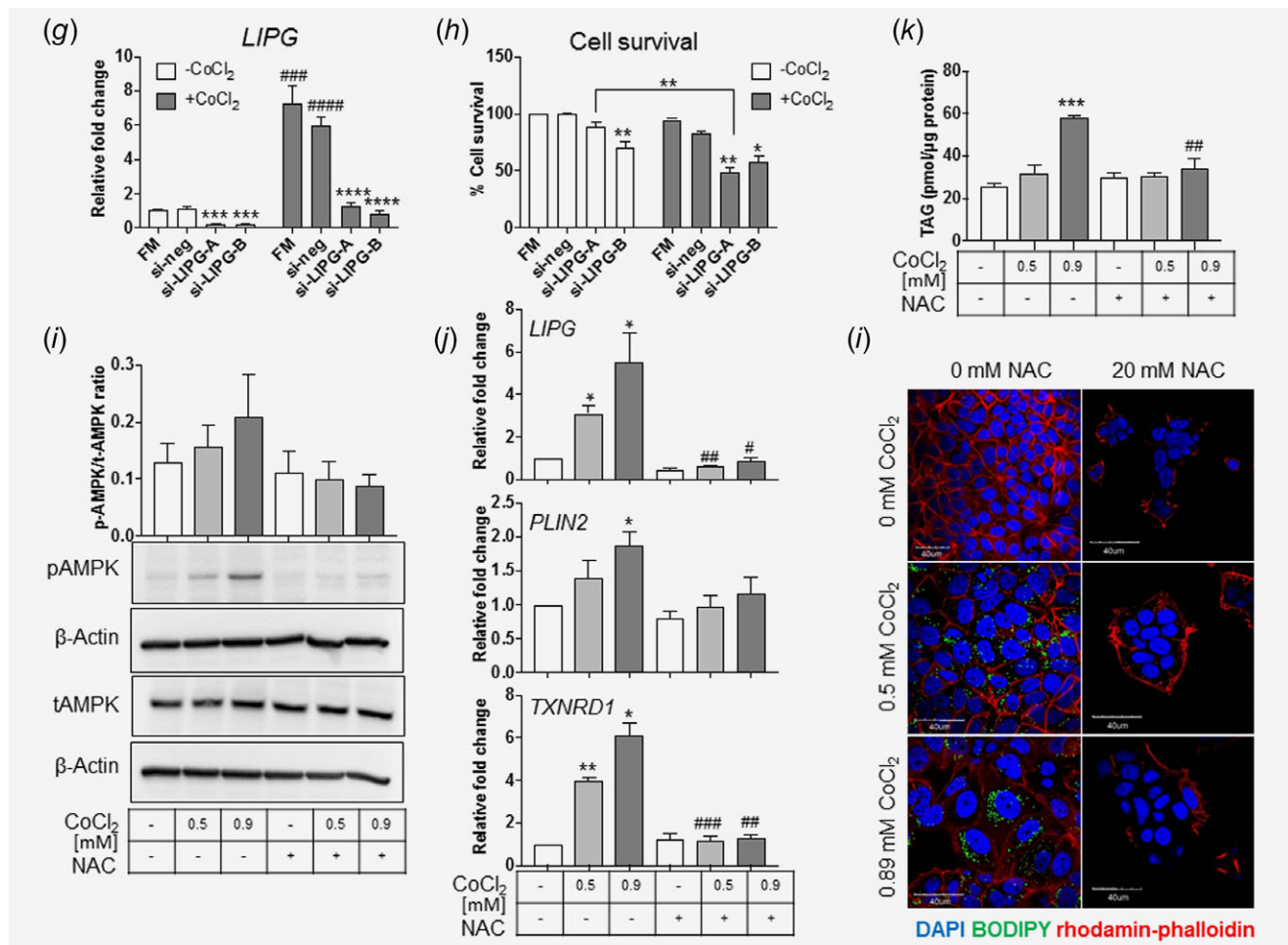


Figure 4. Continued

Next, analysing the association of *LIPG* with MFS in more heterogeneous patient populations, including also node-positive patients and patients who received adjuvant treatment with hormonal drugs and/or chemotherapy revealed a significant association of high *LIPG* expression with worse outcome in one dataset, but was not confirmed to be a general feature of human breast cancer (Figs. S12 and S13, Supporting Information). The lack of association with MFS in tamoxifen-treated breast cancers is however not surprising, since it is in line with our findings that *LIPG* was associated with ER-negative status (Table S6, Supporting Information). That no significant association was observed between high *LIPG* expression and MFS in the datasets where all, or the majority of patients were treated with adjuvant chemotherapy might be due to factors related to the chemotherapy response being more important for metastatic recurrence in an adjuvantly treated patient population.

The previously described *in vitro* experiments demonstrated that *LIPG* supports lipid droplet formation and mitochondrial integrity under conditions of oxidative stress. These findings

were supported in the combined node-negative dataset where the majority of *LIPG*-high tumours also expressed the lipid droplet marker *PLIN2*, and the oxidative stress marker *TXNRD1* at levels above the median (Figs. 5e and 5f). Both *PLIN2* (209122_at) and *TXNRD1* (201266_at) were also significantly associated with shorter MFS in the combined node-negative dataset in a univariate Cox analysis (Tables S7 and S8, Supporting Information), as illustrated by Kaplan–Meier plots (Fig. S14a, Supporting Information) and in previous work.¹¹ However, for the combined node-negative dataset, adding *LIPG* to the model that included *PLIN2* or *TXNRD1* corresponded to a significant increase in the likelihood ratio statistic (Fig. S14b, Supporting Information). This shows that including *LIPG* as a variable adds a significant amount of prognostic information to the model, in addition to *PLIN2* or *TXNRD1*, and is not simply a marker of lipid accumulation. As illustrated by Kaplan–Meier plots, survival was worse when both *PLIN2* and *LIPG* expression were high (Fig. 5g), with similar results being obtained for *LIPG* and *TXNRD1* (Fig. 5h).

In summary, high *LIPG* mRNA expression occurred in a small subset of breast tumours, primarily high grade and ER-negative,

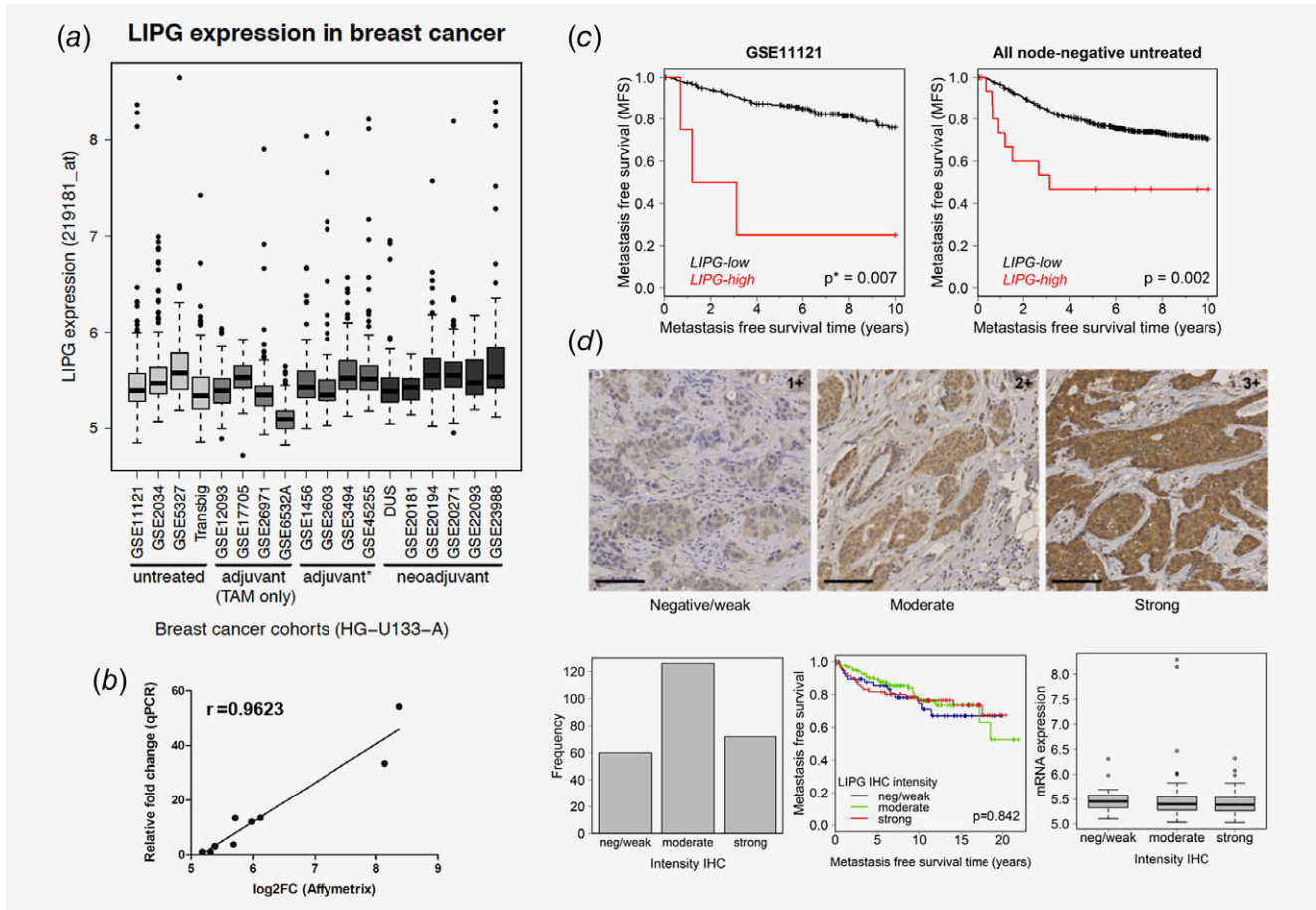


Figure 5. Expression of LIPG in human breast cancer and association with metastasis-free survival. (a) Box plots showing the distribution of LIPG mRNA expression in 18 breast cancer datasets, including node-negative, untreated cohorts as well as cohorts of patients who had received adjuvant (tamoxifen (TAM) only), hormonal and/or chemotherapy and/or both and/or unknown treatment (adjuvant*) and neoadjuvant therapy. (b) Correlation of Affymetrix and qPCR results with Pearson correlation $r = 0.9623$, $p < 0.001$. (c) Kaplan–Meier plots showing association of high LIPG expressing tumours (4 out of 200 tumours using the cut-off $\log_2 \geq 98$ th percentile) with shorter metastasis free survival (MFS) in the Mainz cohort (GSE11121) (left) and in the combined cohort of untreated patients (16 out of 824 tumours, consisting of GSE11121, GSE2034, GSE5327, GSE6532 and GSE7390) (right). p^* : p -Value of the permutation test; p : p -Value from the log-rank test. (d) top: Representative images of LIPG IHC of 259 node-negative breast carcinomas of the tissue microarray (TMA); scale bars: 100 μ m; (d) bottom, left: barplot showing LIPG protein expression distribution in the TMA; (d) bottom, middle: Kaplan–Meier plot of the association of LIPG protein expression (as determined by IHC in the tissue array) with metastasis free survival (MFS). p : p -Value of the log-rank test; (d) bottom right: Association between LIPG mRNA (Affymetrix data) and LIPG protein expression (IHC data) in the Mainz cohort. (e) Scatter plots displaying the relationship between expression of LIPG and PLIN2, and (f) between expression of LIPG and TXNRD1 in the combined cohort of node-negative untreated breast cancer patients. The dashed lines represent the cut-off for LIPG ($\log_2 \geq 98$ th percentile) and the median for PLIN2 and TXNRD1. The number of samples in each quadrant is shown. P : p -Value from Fisher's exact test. (g) Kaplan–Meier plots showing association of LIPG and PLIN2 and (h) LIPG and TXNRD1 with MFS in each of the patient subgroups stratified according to the aforementioned cutpoints. p -Values of the log-rank test for the pairwise comparisons are shown in the corresponding tables. (i) Proposed model: Adaptation of tumour cells to oxidative stress by LIPG: Under normal conditions cells synthesise fatty acids (FA) *de novo* via FAS, which consumes NADPH. Basal levels of LIPG may supply FA as well. Upon oxidative stress, activation of AMPK triggers a metabolic reprogramming that turns down ATP/NADPH consuming pathways such as the *de novo* FAS, enabling NADPH-dependent protein repair via TXNRD1/TXN. Upregulation of LIPG along with PLIN2 and TXNRD1 occurs. Secreted LIPG provides FA that become stored as triglycerides in PLIN2-coated lipid droplets. These support mitochondrial integrity, possibly via lipid remodeling, and thus protect against ROS.

and was associated with shorter MFS in node-negative, systemically untreated tumours. Co-expression of LIPG mRNA with TXNRD1, and PLIN2 suggests a role for LIPG in the context of oxidative stress and lipid droplet accumulation, while simultaneously supporting the results obtained *in vitro*.

Discussion

The present study has uncovered two new aspects of the role of LIPG in breast cancer: First, high LIPG expression, which provides an alternative source of FFA to *de novo* synthesis via extracellular lipolysis, is particularly relevant under oxidative

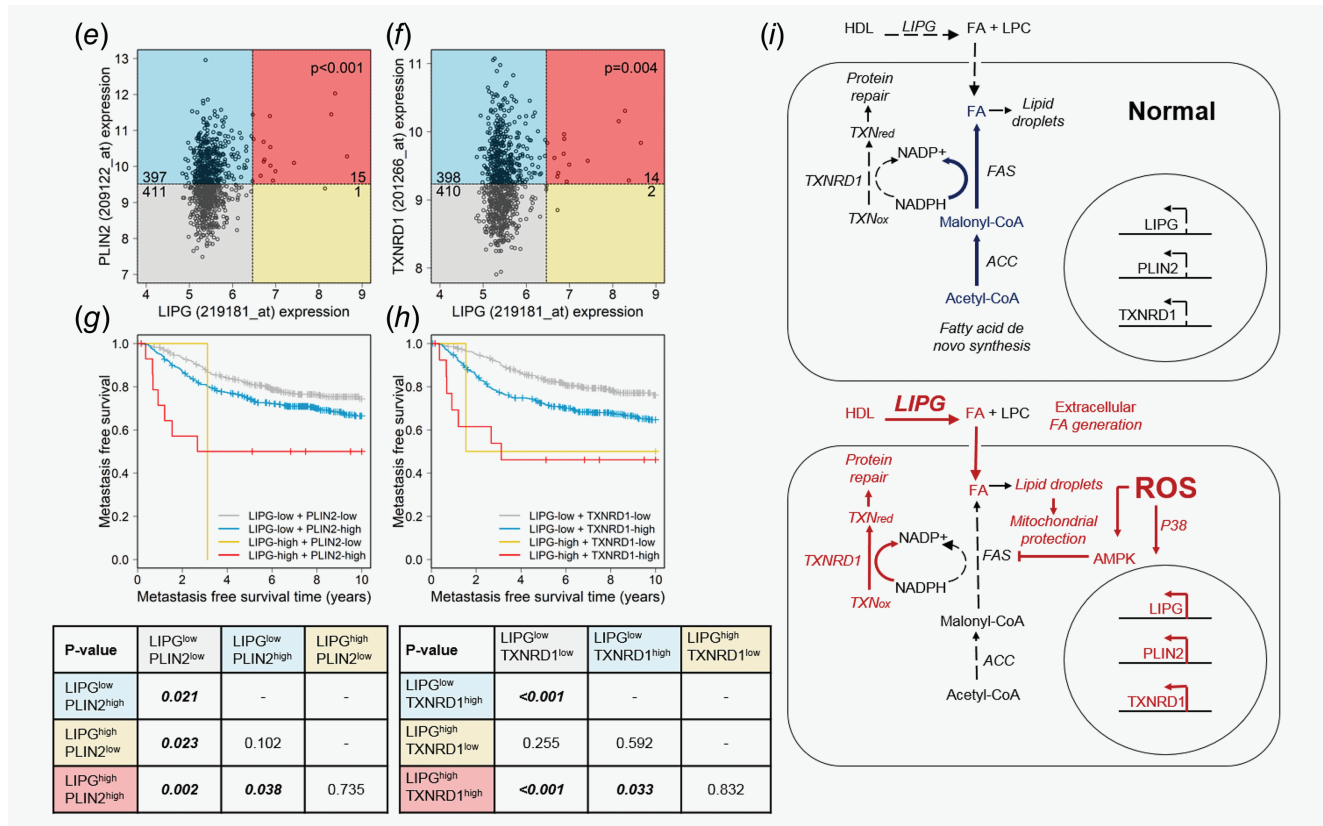


Figure 5. Continued

stress conditions, when lipogenesis is inhibited *via* AMPK. In this context, LDs accumulated by the action of LIPG fuel and protect mitochondria from ROS, possibly superoxide (Fig. 5i). Thus, high compensatory LIPG expression may facilitate tumour cell survival under oxidative stress conditions, which is supported by increased cell death in LIPG-depleted cells. Second, high *LIPG* mRNA expression is significantly associated with shorter MFS of node-negative, adjuvantly untreated breast cancer. Therefore, *LIPG* appears to contribute to unfavourable prognosis, enabling adaptation to oxidative stress.

The different experimental conditions in which we observed *LIPG* upregulation, OIS, chemical hypoxia by CoCl_2 , and exposure to H_2O_2 and rotenone are characterized by severe oxidative stress. This strongly supports oxidative stress as a biological context in which high *LIPG* expression is required for survival of tumour cells. In all cases, increased mRNA levels of *TXNRD1* accompanied the upregulation of *LIPG* expression, indicating an enhanced demand for NADPH-dependent antioxidant pathways. We also showed in two cases that oxidative stress led to a negative regulation of *de novo* FAS *via* AMPK. This mechanism of repression of FAS has been reported to take place under conditions of oxidative stress to avoid consumption of NADPH³⁶ and was also demonstrated to occur in a model

of Ras oncogene-induced senescence in human fibroblasts.³⁷ Since *LIPG*-mediated lipid supply *via* extracellular lipolysis is NADPH-independent, we propose that this alternative pathway reduces NADPH consumption, which then is available as a cofactor of *TXNRD1* for protein repair (Fig. 5i).

It is noteworthy that although hypoxia-induced oxidative stress has been reported to upregulate a pathway of exogenous FFA uptake due to a compromised *de novo* FAS³⁸ our study showed that *LIPG* is not upregulated by hypoxia (1% O_2). This suggests that *LIPG* is not essential in hypoxia-triggered lipid accumulation under these conditions.

Our findings also indicate that FFAs supplied by LIPG contribute to the formation of LDs. Lipid droplets have recently been reported to protect cells against ROS.^{38,39} One potential mechanism is the redirection of ROS-susceptible polyunsaturated fatty acids from the cell membrane to LDs where they are shielded from peroxidation.³⁹ Interestingly, our previous study showed that senescent MCF-7/NeuT cells underwent a glycerophospholipid remodelling towards increased saturation of acyl chains, thereby decreasing susceptibility to peroxidation.⁸ In this context, LIPG-triggered LDs may support membrane lipid repair, preserving mitochondrial integrity from ROS. Thus, in contrast to a reported role for LIPG in fuelling proliferation,⁹

Table 1. Univariate and multivariate Cox analysis showing association of *LIPG* mRNA expression with metastasis free survival (MFS) in a combined cohort of node-negative untreated breast cancer patients (n = 824) consisting of the GSE11121 (n = 200), GSE2034, (n = 286), Transbig (GSE6532 and GSE7390, n = 280) and GSE5327 (n = 58) cohorts

Combined cohort						
	Univariate			Multivariate		
	HR	p	95% CI	HR	p	95% CI
Age						
<50 years	1.00			1.00		
≥50 years	1.01	0.976	0.71–1.43	1.02	0.922	0.71–1.47
pT stage						
Stage I	1.00			1.00		
Stage II + III	1.32	0.114	0.93–1.87	1.18	0.370	0.82–1.71
Grade						
Grade 1 + 2	1.00			1.00		
Grade 3	1.93	<0.001	1.36–2.75	1.70	0.013	1.12–2.58
ER status						
Negative	1.00			1.00		
Positive	0.74	0.031	0.56–0.97	1.00	0.987	0.64–1.57
HER2 status						
Negative	1.00			1.00		
Positive	1.13	0.468	0.81–1.58	1.20	0.465	0.74–1.93
<i>LIPG</i>	1.59	0.002	1.18–2.15	1.95	0.002	1.26–2.99

Abbreviations: HR, hazard ratio; p, p-value (unadjusted); CI, confidence interval.

the present results showed a cell proliferation-independent and previously unrecognized role of *LIPG* in enabling protective LDs accumulation in tumour cells. In agreement with this hypothesis, breast tumours expressing high levels of *LIPG* also expressed high levels of the oxidative stress marker *TXNRD1*, and the lipid droplet marker *PLIN2* and MFS time was shorter in *PLIN2* and *LIPG*-high as well as in *TXNRD1* and *LIPG*-high subgroups compared to only-*TXNRD1*-high or only-*PLIN2*-high subgroups. The finding that *LIPG* significantly improved the likelihood ratio statistics compared to models with *PLIN2* or *TXNRD1* alone demonstrates the independent contribution of *LIPG* to worse prognosis.

Our findings that high *LIPG* mRNA expression is restricted in breast cancer and significantly associated with worse survival apparently contradict the study reporting a broad expression and no significant association between IHC-determined *LIPG* and survival.⁹ When we performed IHC of our TMA, using the same *LIPG* antibody as Slebe and co-workers,⁹ we also found no association of cytoplasmic *LIPG* positivity with prognosis in our cohort, but also no association of cytoplasmic *LIPG* positivity with *LIPG* transcript levels. Importantly, our *in vitro* studies demonstrated that *LIPG* mRNA levels only correlated with those of extracellular *LIPG* protein and not with those of cytoplasmic *LIPG*, which may account for the remaining non-secreted *LIPG* pool. Since the extracellular localization

enables *LIPG* to access serum lipoproteins for lipid supply we conclude that the actively secreted *LIPG* protein, and thus, as a surrogate, *LIPG* transcript levels represent a more relevant measure for analysing the association with tumour prognosis. Notably, only *via* this approach could *LIPG*'s association with worse prognosis be uncovered. The initial observation of *LIPG*'s association with shorter MFS made in our own cohort was subsequently confirmed in two additional publicly available breast cancer cohorts. Moreover, a significant association of high *LIPG* with grade 3 and with negative ER status was observed. The latter was in agreement with a much higher *LIPG* expression in the triple negative cell lines MDA-MB231 and MDA-MB468, and in the ER-/HER2+ cell lines HCC1954 and SKBR3 than in the ER-positive cell lines MCF-7, T47D and BT474. The lack of significant association of high *LIPG* with HER2 status observed in tumours and in the cell lines was consistent with our finding that *LIPG* is not upregulated by HER2 overexpression in cultured breast cancer cells. Finally, our findings are in line with a recent study reporting expression and a role for *LIPG* in metastasis of human basal-like triple-negative breast cancer.¹⁰

In summary, integrating our *in vitro* experimental data and our analysis of *LIPG*-expressing tumours led to the concept that *LIPG* upregulation in cancer cells under oxidative stress enables survival when the lipid requirement of the cell exceeds its capacity to synthesize fatty acids *de*

nov, or when *de novo* lipogenesis is repressed by ROS. Although cancer cells have generally high ROS levels, these levels further increase under a harsh tumour microenvironment, nutrient deprivation or upon matrix detachment.^{40,41} Thus, metabolic adaptation to these conditions *via* LIPG upregulation may be a crucial event determining adverse progression, as suggested by the observation that high LIPG expression is associated with shorter MFS.

References

- Santos CR, Schulze A. Lipid metabolism in cancer. *FEBS J* 2012;279:2610–23.
- Zaidi N, Lupien L, Kuemmerle NB, et al. Lipogenesis and lipolysis: the pathways exploited by the cancer cells to acquire fatty acids. *Prog Lipid Res* 2013;52:585–9.
- Kuhajda FP. Fatty acid synthase and cancer: new application of an old pathway. *Cancer Res* 2006;66:5977–80.
- Kuemmerle NB, Rysman E, Lombardo PS, et al. Lipoprotein lipase links dietary fat to solid tumor cell proliferation. *Mol Cancer Therap* 2011;10:427–36.
- Jaye M, Lynch KJ, Krawiec J, et al. A novel endothelial-derived lipase that modulates HDL metabolism. *Nat Genet* 1999;21:424–8.
- Choi SY, Hirata K, Ishida T, et al. Endothelial lipase: a new lipase on the block. *J Lipid Res* 2002;43:1763–9.
- Riederer M, Kofeler H, Lechleitner M, et al. Impact of endothelial lipase on cellular lipid composition. *Biochim Biophys Acta* 2012;1821:1003–11.
- Cadenas C, Vosbeck S, Hein EM, et al. Glycerophospholipid profile in oncogene-induced senescence. *Biochim Biophys Acta* 2012;1821:1256–68.
- Slebe F, Rojo F, Vinaixa M, et al. FoxA and LIPG endothelial lipase control the uptake of extracellular lipids for breast cancer growth. *Nat Commun* 2016;7:11199.
- Lo PK, Yao Y, Lee JS, et al. LIPG signaling promotes tumor initiation and metastasis of human basal-like triple-negative breast cancer. *Elife* 2018;7:e31334.
- Cadenas C, Franckenstein D, Schmidt M, et al. Role of thioredoxin reductase 1 and thioredoxin interacting protein in prognosis of breast cancer. *Breast Cancer Res* 2010;12:R44.
- Trost TM, Lausch EU, Fees SA, et al. Premature senescence is a primary fail-safe mechanism of ERBB2-driven tumorigenesis in breast carcinoma cells. *Cancer Res* 2005;65:840–9.
- Greulich H, Kaplan B, Mertins P, et al. Functional analysis of receptor tyrosine kinase mutations in lung cancer identifies oncogenic extracellular domain mutations of ERBB2. *Proc Natl Acad Sci USA* 2012;109:14476–81.
- Koopman R, Schaart G, Hesselink MK. Optimisation of oil red O staining permits combination with immunofluorescence and automated quantification of lipids. *Histochem Cell Biol* 2001;116:63–8.
- Livak KJ, Schmittgen TD. Analysis of relative gene expression data using real-time quantitative PCR and the 2[−](Delta Delta C(T)) method. *Methods* 2001;25:402–8.
- Barrett T, Wilhite SE, Ledoux P, et al. NCBI GEO: archive for functional genomics data sets--update. *Nucleic Acids Res* 2013;41:D991–5.
- McCall MN, Bolstad BM, Irizarry RA. Frozen robust multiarray analysis (fRMA). *Biostatistics* 2010;11:242–53.
- Uhlen M, Zhang C, Lee S, et al. A pathology atlas of the human cancer transcriptome. *Science (New York, NY)* 2017;357:eaan2507.
- Gauster M, Hrzanjak A, Schick K, et al. Endothelial lipase is inactivated upon cleavage by the members of the proprotein convertase family. *J Lipid Res* 2005;46:977–87.
- Gauster M, Rechberger G, Sovic A, et al. Endothelial lipase releases saturated and unsaturated fatty acids of high density lipoprotein phosphatidylcholine. *J Lipid Res* 2005;46:1517–25.
- Nomura DK, Casida JE. Lipases and their inhibitors in health and disease. *Chem Biol Interact* 2016;259:211–22.
- Wang SE, Narasanna A, Perez-Torres M, et al. HER2 kinase domain mutation results in constitutive phosphorylation and activation of HER2 and EGFR and resistance to EGFR tyrosine kinase inhibitors. *Cancer Cell* 2006;10:25–38.
- Pizer ES, Thupari J, Han WF, et al. Malonyl-coenzyme-a is a potential mediator of cytotoxicity induced by fatty-acid synthase inhibition in human breast cancer cells and xenografts. *Cancer Res* 2000;60:213–8.
- Ruderman NB, Cacicedo JM, Itani S, et al. Malonyl-CoA and AMP-activated protein kinase (AMPK): possible links between insulin resistance in muscle and early endothelial cell damage in diabetes. *Biochem Soc Trans* 2003;31:202–6.
- Park H, Kaushik VK, Constant S, et al. Coordinate regulation of malonyl-CoA decarboxylase, sn-glycerol-3-phosphate acyltransferase, and acetyl-CoA carboxylase by AMP-activated protein kinase in rat tissues in response to exercise. *J Biol Chem* 2002;277:32571–7.
- Moiseeva O, Bourdeau V, Roux A, et al. Mitochondrial dysfunction contributes to oncogene-induced senescence. *Mol Cell Biol* 2009;29:4495–507.
- Zechner R, Zimmermann R, Eichmann TO, et al. FAT SIGNALS--lipases and lipolysis in lipid metabolism and signaling. *Cell Metab* 2012;15:279–91.
- Rambold AS, Cohen S, Lippincott-Schwartz J. Fatty acid trafficking in starved cells: regulation by lipid droplet lipolysis, autophagy, and mitochondrial fusion dynamics. *Dev Cell* 2015;32:678–92.
- Yu J, Zhang S, Cui L, et al. Lipid droplet remodeling and interaction with mitochondria in mouse brown adipose tissue during cold treatment. *Biochim Biophys Acta* 2015;1853:918–28.
- Adam T, Opie LH, Essop MF. AMPK activation represses the human gene promoter of the cardiac isoform of acetyl-CoA carboxylase: role of nuclear respiratory factor-1. *Biochem Biophys Res Commun* 2010;398:495–9.
- Marques AP, Rosmaninho-Salgado J, Estrada M, et al. Hypoxia mimetic induces lipid accumulation through mitochondrial dysfunction and stimulates autophagy in murine preadipocyte cell line. *Biochim Biophys Acta (BBA)-Gen Sub* 2017;1861:673–82.
- Lee AC, Fenster BE, Ito H, et al. Ras proteins induce senescence by altering the intracellular levels of reactive oxygen species. *J Biol Chem* 1999;274:7936–40.
- Catalano A, Rodilossi S, Caprari P, et al. 5-Lipoxygenase regulates senescence-like growth arrest by promoting ROS-dependent p53 activation. *EMBO J* 2005;24:170–9.
- Schmidt M, Bohm D, von Torne C, et al. The humoral immune system has a key prognostic impact in node-negative breast cancer. *Cancer Res* 2008;68:5405–13.
- Schmidt M, Hellwig B, Hammad S, et al. A comprehensive analysis of human gene expression profiles identifies stromal immunoglobulin kappa C as a compatible prognostic marker in human solid tumors. *Clin Cancer Res* 2012;18:2695–703.
- Jeon SM, Chandel NS, Hay N. AMPK regulates NADPH homeostasis to promote tumour cell survival during energy stress. *Nature* 2012;485:661–5.
- Quijano C, Cao L, Fergusson MM, et al. Oncogene-induced senescence results in marked metabolic and bioenergetic alterations. *Cell Cycle* 2012;11:1383–92.
- Bensaad K, Favaro E, Lewis CA, et al. Fatty acid uptake and lipid storage induced by HIF-1alpha contribute to cell growth and survival after hypoxia-reoxygenation. *Cell Rep* 2014;9:349–65.
- Bailey AP, Koster G, Guillemier C, et al. Antioxidant role for lipid droplets in a stem cell niche of drosophila. *Cell* 2015;163:340–53.
- Galadari S, Rahman A, Pallichankandy S, et al. Reactive oxygen species and cancer paradox: to promote or to suppress? *Free Radic Biol Med* 2017;104:144–64.
- DeBerardinis RJ, Chandel NS. Fundamentals of cancer metabolism. *Sci Adv* 2016;2:e1600200.

24 days of stem cells

Shape the future of stem cell innovation
October 1- November 1, 2019

Join us for 24 Days of Stem Cells; a premiere virtual event featuring the latest advances in stem cell research.

This year's format will feature a new hour of cutting edge content every week day starting October 1st. Attend the sessions that are most relevant to your work - at your convenience and at your pace.

During the 24-day long event, you can:

- Access leading scientific presentations from thought leaders around the world
- Watch live training demonstrations from our stem cell experts
- Download key stem cell tools and resources
- Complete weekly challenges to earn points towards certification and prizes

Register today at
www.24daysofstemcells.com

ThermoFisher
SCIENTIFIC

WILEY